Monthly Notices
of the
ROYAL ASTRONOMICAL SOCIETY

MNRAS **456,** 1595–1606 (2016) doi:10.1093/mnras/stv2813

The SDSS-III BOSS quasar lens survey: discovery of 13 gravitationally lensed quasars

Anupreeta More,[1⋆] Masamune Oguri,[1,2,3⋆] Issha Kayo,[4] Joel Zinn,[5,6] Michael A. Strauss,[6] Basilio X. Santiago,[7,8] Ana M. Mosquera,[5,9] Naohisa Inada,[10] Christopher S. Kochanek,[5,11] Cristian E. Rusu,[12,13,14] Joel R. Brownstein,[15] Luiz N. da Costa,[8,16] Jean-Paul Kneib,[17,18] Marcio A. G. Maia,[8,16] Robert M. Quimby,[1,19] Donald P. Schneider,[20,21] Alina Streblyanska[22,23] and Donald G. York[24,25]

[1]*Kavli Institute for the Physics and Mathematics of the Universe (Kavli IPMU, WPI), University of Tokyo, Chiba 277-8583, Japan*
[2]*Research Center for the Early Universe, University of Tokyo, 7-3-1 Hongo, Bunkyo-ku, Tokyo 113-0033, Japan*
[3]*Department of Physics, University of Tokyo, 7-3-1 Hongo, Bunkyo-ku, Tokyo 113-0033, Japan*
[4]*Department of Liberal Arts, Tokyo University of Technology, 5-23-22 Nishikamata, Ota-ku, Tokyo 114-8650, Japan*
[5]*Department of Astronomy, The Ohio State University, 140 West 18th Avenue, Columbus, OH 43210, USA*
[6]*Princeton University Observatory, Peyton Hall, Princeton, NJ 08544, USA*
[7]*Instituto de Física, UFRGS, CP 15051, Porto Alegre, RS 91501970, Brazil*
[8]*Laboratório Interinstitucional de e-Astronomia-LIneA, Rua General José Cristino 77, Rio de Janeiro, RJ 20921-400, Brazil*
[9]*Physics Department, United States Naval Academy, Annapolis, MD 21403, USA*
[10]*Department of Physics, Nara National College of Technology, Yamatokohriyama, Nara 639-1080, Japan*
[11]*Center for Cosmology and AstroParticle Physics (CCAPP), The Ohio State University, 191 W. Woodruff Ave, Columbus, OH 43210, USA*
[12]*Department of Physics, University of California, Davis, CA 95616, USA*
[13]*Optical and Infrared Astronomy Division, National Astronomical Observatory of Japan, 2-21-1, Osawa, Mitaka, Tokyo 181-8588, Japan*
[14]*Department of Astronomy, University of Tokyo, 7-3-1 Hongo, Bunkyo-ku, Tokyo 113-0033, Japan*
[15]*Department of Physics and Astronomy, University of Utah, 115 S. 1400 E., Salt Lake City, UT 84112, USA*
[16]*Observatório Nacional, Rua General José Cristino 77, Rio de Janeiro, RJ 20921-400, Brazil*
[17]*Ecole Polytechnique Fédérale de Lausanne (EPFL), Observatoire de Sauverny, CH-1290 Versoix, Switzerland*
[18]*Aix Marseille Université, CNRS, LAM (Laboratoire d'Astrophysique de Marseille) UMR 7326, F-13388 Marseille, France*
[19]*Department of Astronomy, San Diego State University, San Diego, CA 92182, USA*
[20]*Department of Astronomy and Astrophysics, The Pennsylvania State University, University Park, PA 16802, USA*
[21]*Institute for Gravitation and the Cosmos, The Pennsylvania State University, University Park, PA 16802, USA*
[22]*Instituto de Astrofísica de Canarias (IAC), E-38200 La Laguna, Tenerife, Spain*
[23]*Universidad de La Laguna (ULL), Dept. Astrofísica, E-38206 La Laguna, Tenerife, Spain*
[24]*The University of Chicago, 5640 South Ellis Avenue, Chicago, IL 60637, USA*
[25]*The Enrico Fermi Institute, 5640 South Ellis Avenue, Chicago, IL 60637, USA*

Accepted 2015 November 27. Received 2015 November 3; in original form 2015 September 25

ABSTRACT

We report the discovery of 13 confirmed two-image quasar lenses from a systematic search for gravitationally lensed quasars in the SDSS-III Baryon Oscillation Spectroscopic Survey (BOSS). We adopted a methodology similar to that used in the SDSS Quasar Lens Search (SQLS). In addition to the confirmed lenses, we report 11 quasar pairs with small angular separations ($\lesssim$2 arcsec) confirmed from our spectroscopy, which are either projected pairs, physical binaries, or possibly quasar lens systems whose lens galaxies have not yet been detected. The newly discovered quasar lens system, SDSS J1452+4224 at $z_s \approx 4.8$ is one of the highest redshift multiply imaged quasars found to date. Furthermore, we have over 50 good lens candidates yet to be followed up. Owing to the heterogeneous selection of BOSS quasars, the lens sample presented here does not have a well-defined selection function.

Key words: gravitational lensing: strong – methods: statistical.

⋆E-mail: anupreeta.more@ipmu.jp (AM); masamune.oguri@ipmu.jp (MO)

1 INTRODUCTION

Gravitationally lensed quasars provide a unique tool to study the Universe. In particular, the time-variable nature of quasars enable us to measure the arrival time difference between quasar multiple images, which may be a powerful probe of cosmology (e.g. Refsdal 1964; Schechter et al. 1997; Treu et al. 2013). Applications of gravitationally lensed quasars such as time delay cosmography (e.g. Coles 2008; Suyu et al. 2010), constraints on the quasar luminosity function (e.g. Comerford, Haiman & Schaye 2002; Richards et al. 2006), constraints on dark energy (e.g. Kochanek 1996; Oguri et al. 2012), and study of the host galaxy and/or black hole properties (e.g. Peng et al. 2006; Mosquera et al. 2013; Rusu et al. 2015) are still limited by small number statistics, indicating the importance of finding new gravitationally lensed quasars in wide-field surveys.

The SDSS Quasar Lens Search (SQLS; Oguri et al. 2006, 2008, 2012; Inada et al. 2008, 2010, 2012) considerably advanced the field by discovering nearly 50 new quasar lenses. The SQLS was based upon the large sample of spectroscopically confirmed quasars in the Sloan Digital Sky Survey – I/II (SDSS; York et al. 2000). Candidates were first selected from the ∼100 000 spectroscopic quasars and their SDSS images were then examined to identify quasars with extended morphology or with nearby companion objects of similar colour. The lens candidates were then confirmed with various facilities to construct a secure sample of gravitationally lensed quasars. Thanks to the well-studied selection function (Oguri et al. 2006), a subsample of the SQLS quasar lenses was used to place statistical limits on dark energy and the evolution of massive galaxies that act as lenses (Oguri et al. 2012).

The Baryon Oscillation Spectroscopic Survey (BOSS; Dawson et al. 2013) of the SDSS-III (Eisenstein et al. 2011) is a new spectroscopic survey to measure the expansion rate of the Universe. In addition to an extensive spectroscopic survey of $z \sim 0.5$ galaxies, BOSS has obtained spectra of ∼300 000 quasars (Alam et al. 2015) with over 180 000 in the redshift range $2.15 < z < 4$ in order to detect baryon acoustic oscillation signatures in the Ly α absorption features of their spectra. The large number of BOSS quasars suggests that it should contain a large number of gravitationally lensed quasars. However, the lensing rate of the BOSS quasar sample is likely smaller than that of the SDSS-II quasar sample because BOSS largely targets point-like quasar candidates in order to increase the survey efficiency. In this case, lensed quasars where the images are not individually resolved would appear extended and would tend to be excluded by the BOSS selection function. On the other hand, the typical BOSS quasar is at a higher redshift ($z \sim 2$–3 Ross et al. 2012; Pâris et al. 2014) than the typical SDSS-I/II quasars ($z \sim$ 1–2) and this higher average redshift may partly compensate for the lower lensing rate due to the morphological target selection.

We thus started a new survey for gravitationally lensed quasars from BOSS called the BOSS quasar lens survey (BQLS). The basic strategy follows that of the SQLS in that we select quasar lens candidates by examining the SDSS images of BOSS quasars and conduct additional observations of any promising quasar lens candidates. In this paper, we present 13 confirmed quasar lenses from the BQLS. In addition, we also identify 11 quasar close pairs with not quite identical but similar spectra. Some of these may be true gravitational lenses but could not be confirmed due to lack of detection of a lens galaxy or spectra being slightly different due to effects such as microlensing and dust extinction.

This paper is organized as follows. In Section 2, we describe the selection of our lens candidates. In Section 3, we describe the additional observations undertaken for a detailed examination of the most promising lens candidates. The mass modelling of the lenses is described in Section 4. We compare the confirmed lenses to the SQLS lens sample and present our general findings in Section 5. Section 6 presents our summary and conclusions.

2 CANDIDATE SELECTION

We selected candidate quasar lens systems from the imaging and spectroscopic data of SDSS-III/BOSS. The SDSS uses a dedicated 2.5-metre telescope at Apache Point Observatory in New Mexico (Gunn et al. 2006). The SDSS imaging data uses five (*ugriz*) broad-band filters and has a limiting magnitude of $r \sim 22.5$, which were used to select various targets including quasars for spectroscopic observations (Ross et al. 2012). The SDSS-III/BOSS survey uses an upgraded multi-object fibre spectrograph which can simultaneously take spectra of 1000 objects with a resolving power $R \sim 2000$ and a wavelength coverage of $3600 < \lambda < 10\,400$ Å (Smee et al. 2013).

We largely followed the procedures established in the SQLS for the lens candidate selection process. In the SQLS, however, there were also image separation and flux ratio limits for constructing a complete lens sample for statistical studies. In SDSS-III, constructing a well-defined statistical sample is much more challenging because of the complex nature of the quasar target selection (Ross et al. 2012). Thus, we first adopted a simple approach of applying the SQLS-like selection criteria and then choosing the best lens candidates by visually inspecting the SDSS images of all of the resulting lens candidates. Below we describe these procedures in more detail.

The selection method for the underlying SDSS-III/BOSS spectroscopic quasar sample is presented in Ross et al. (2012) and Pâris et al. (2014). Currently all of the BOSS data are public, and the quasar catalogue we used is available at http://www.sdss.org/dr12/algorithms/boss-dr12-quasar-catalog/. From the spectroscopic quasar catalogue, we selected quasar lens candidates using a method similar to SQLS, in which morphological and colour criteria were used to select lens candidates from the object catalogue. The full details of the SQLS selection algorithm are presented in Oguri et al. (2006) and Inada et al. (2008). While the SQLS selection criteria were optimized for selecting low-redshift ($z < 2.2$) quasar lens candidates, an extension of the selection algorithm to higher redshifts is discussed in Inada et al. (2009). In this paper, we adopted a modified version of these morphological and colour selection criteria as described below.

The morphological selection approach identified spectroscopic quasars that are poorly fit by the imaging point spread function (PSF). Even though BOSS targeted point-like quasars, there are extended objects with a spectroscopic classification of a quasar in BOSS which were originally identified as galaxies and targeted as part of the galaxy follow-up programmes or ancillary programmes targeting AGNs. Therefore, we applied the morphological selection to find small image separation lensed quasars which appear as extended quasar-like sources. Specifically, we used the following object parameters; `type`, which describes the classification of objects as stars (`type` = 6) or galaxies (`type` = 3); `lnlStar`, which is the logarithm of the likelihood of objects being fitted by the PSF of the field; `lnlDeV`, which is the logarithm of the likelihood of objects being fitted by the de Vaucouleurs profile. The parameters `lnlStar` and `lnlDeV` are available for each broad-band. For quasars at $0.7 < z < 3$, we selected lens candidates whose *gri*-band object parameters satisfy `lnlStar` < -1 for `type` = 3 and `lnlDeV` < -15 and `lnlStar` − `lnlDeV` < -5 for `type` = 6. For quasars at $z > 3$, we used the same criteria as above but only for

the r and i bands. There were ∼3000 candidates selected by these criteria.

For a given spectroscopic quasar, the colour selection method searches for nearby objects with similar colours out to a maximum image separation of $\Delta\theta = 30$ arcsec. For quasars at $0.7 < z < 3.4$, we used all five bands and select objects with colour differences smaller than 0.1 for $g - r$ and $r - i$ and smaller than 0.2 for $u - g$ and $i - z$, where the colours were computed using PSF magnitudes. For quasars at $z > 3.4$, we used only the *griz*-bands and similar thresholds for the colour differences of 0.1 for $r - i$ and 0.2 for $g - r$ and $i - z$. We also required that the i-band magnitude difference of the two objects was smaller than 1. When the angular separation of the two objects were small (<3.5 arcsec), we used relaxed colour criteria as the SDSS photometry might not be reliable (see Oguri et al. 2006). This colour selection method led to a sample of ∼2000 candidates.

We then visually inspected all the morphological and colour selected lens candidates. The visual inspection was performed by one of the authors (MO) to define 'good' lens candidates that have relatively high chance of being true lens systems. Here, the goodness of the candidates was judged by various factors including the presence of multiple components with quasar-like colours or nearby galaxies that might act as lenses. Most of the false positives removed in the visual inspection are either single quasars with contamination from bright nearby objects and obvious quasar-galaxy superpositions. Large-separation ($\gtrsim$5 arcsec) quasar lenses are much less common, and hence large-separation lens candidates are not regarded as good unless putative lens galaxies or clusters are seen in between the candidate quasar images. We finally selected ∼80 good candidates and an additional ∼70 possible lens candidates from the morphological selection, and ∼75 good candidates and ∼65 possible lens candidates from the colour selection. There is an overlap of ∼20 good candidates between the morphology and colour selected samples. The number of lens candidates, requiring observational follow-up studies was reduced by a factor of ∼20 through the visual inspection. This suggests that our approach is an efficient approach to find the most promising lens candidates. Nevertheless, it is possible that we missed some true gravitational lens systems in the course of the visual inspection. For example, we are likely to miss quasars that are fainter and do not visually look star-like which includes some small image-separation lenses and possibly quadruply imaged systems. We may also have missed systems with atypical image configurations, odd colours or highly anomalous flux ratios.

We note that Dahle et al. (2013, 2015) discovered a gravitationally lensed sextuple quasar with a maximum image separation of 15.1 arcsec, SDSS J2222+2745, from the SDSS-III data. They searched for strong lens candidates by visually inspecting photometrically identified clusters of galaxies. Even though this lens system meets our image separation criteria, none of the lensed quasars from SDSS J2222+2745 were selected for spectroscopy by BOSS so this source is not in our parent sample.

Some gravitationally lensed quasars have been discovered by identifying quasar spectral features superposed on the spectra of lens galaxies (e.g. Johnston et al. 2003; Bolton et al. 2005; McGreer et al. 2010) although this technique of identifying compound objects spectroscopically has primarily discovered many examples of lensed star-forming galaxies (e.g. Bolton et al. 2006b). As a complementary approach to the SQLS selection technique, we also searched for lensed quasars using this technique. We identified instances of quasar-galaxy superpositions in the BOSS spectra with quasars at $z < 5.5$ and galaxies with redshifts lower than the quasars (Zinn et al., in preparation). The initial sample had 17 good candidates out of which three systems were followed-up spectroscopically as part of the BQLS sample. Currently, this search has produced ∼100 candidates with a 'good' visual quality flag and will be presented in Zinn et al. (in preparation).

The BOSS DR12 catalogue has some known lenses, several of which are in the SQLS. This known sample was excluded prior to the visual inspection of the candidates. In total, we identified about 250 new lens candidates for further study. In the next section, we present initial follow-up results of the most promising quasar lens candidates.

3 DATA: OBSERVATION, REDUCTION AND ANALYSIS

Our follow-up observations consist of imaging and spectroscopic observations. We first attempt to obtain follow-up images for the good lens candidates, and conduct follow-up spectroscopic observations only when the follow-up images show evidence for gravitational lensing. However, it was not possible to follow this strategy strictly due to observing constraints. In some cases, we obtained follow-up spectra before we conducted imaging follow-up observations. Among these systems, those with clear differences in the spectra were thus not observed with imaging. Since the spectroscopic observations are very informative for confirming or ruling out the lensing hypotheses of the candidates, below we first present the complete spectroscopic follow-up results for the best 55 candidates, and then present imaging follow-up results for confirmed gravitational lens systems. The full imaging follow-up results will be presented in an upcoming paper.

3.1 Spectroscopy

Table 1 summarizes our spectroscopic observations. We obtained spectra of five candidates with the Low Resolution Imaging Spectrometer (LRIS; Oke et al. 1995) on the Keck telescope on 2013 September 7. We used the 1.0 arcsec slit, the 400/3400 grism for the blue channel and the 400/8500 grating for the red channel. The spectral resolution was $R \sim 600$ in the blue channel and $R \sim 1300$ in the red channel. The red channel was binned to give 0.27 arcsec pixel^{-1}. The unbinned blue channel has 0.135 arcsec pixel^{-1}. We also obtained spectra of 50 candidates with the Faint Object Camera and Spectrograph (FOCAS; Kashikawa et al. 2002) on the Subaru telescope on 2014 May 2, 2015 Feb 19, and 2015 June 19. In all of the FOCAS observations we used the 1.0 arcsec slit, but adopted two different configurations depending on the quasar redshifts; one is the grism and filter set of 300B/L600 to cover the wavelength range of 3700–6000 Å, and the other is 300B/SY47 4700–9100 Å. Both data sets have a spectral resolution of $R \sim$ 400–500. The data were binned 2 × 2 on the detector, providing a spatial resolution of 0.21 arcsec pixel^{-1}. In all of the observations, the long-slit was aligned to observe both putative quasar images simultaneously. The data were reduced using standard IRAF[1] tasks.

We found that 13 out of the 55 quasar lens candidates contain two quasar components with identical redshifts and similarities in the spectral energy distributions (SEDs). Together with the analysis of the imaging observations presented below, we conclude that these

[1] IRAF is distributed by the National Optical Astronomy Observatories, which are operated by the Association of Universities for Research in Astronomy, Inc., under cooperative agreement with the National Science Foundation.

Table 1. Summary of spectroscopic observations. The 'Selection' column indicates the method(s) with 'M' for morphological selection, 'C' for colour selection, and 'S' for spectroscopic selection (see the text for details). Several candidates were selected by multiple methods. 'Observation' indicates the telescope (S-Subaru or K-Keck), the date and setup of the spectroscopic observations (see also Section 3.1). 'Result' indicates the conclusion from the follow-up spectroscopy as well as imaging observations described in Section 3.2. The $z_{\rm QSO}$ are taken from the BOSS DR12 catalogue which has redshifts corrected after visual inspection of the spectra. The last column has redshifts from the follow-up spectra except when marked with[a] which are taken from the BOSS spectrum.

Object ID	RA (J2000)	Dec. (J2000)	Selection	$z_{\rm QSO}$	Observation	Exp. (s)	Result
SDSS J0033+2015	00:33:37.59	+20:15:38.2	C	2.701	K, 2013 Sep (400/3400+400/8500)	600	Quasar+star
SDSS J0035+2659	00:35:31.98	+26:59:59.9	M	2.294	S, 2015 Jun (300B/L600)	1500	Different SED
SDSS J0114+0722	01:14:38.38	+07:22:28.5	MC	1.828	K, 2013 Sep (400/3400+400/8500)	600	**Quasar lens** ($z_l = 0.408$)
SDSS J0139+1908	01:39:40.69	+19:08:40.7	MC	3.095	K, 2013 Sep (400/3400+400/8500)	600	Different SED
SDSS J0206+0440	02:06:49.50	+04:40:19.0	C	2.396	K, 2013 Sep (400/3400+400/8500)	600	Different SED
SDSS J0213−0421	02:13:22.86	−04:21:34.3	C	1.910	S, 2015 Feb (300B/L600)	900	Quasar pair $z = 1.911$&0.992
SDSS J0256+0153	02:56:40.76	+01:53:29.3	S	2.600	K, 2013 Sep (400/3400+400/8500)	600	**Quasar lens** ($z_l = 0.603$)
SDSS J0737+4825	07:37:08.67	+48:25:51.1	M	2.892	S, 2015 Feb (300B/L600)	1080	**Quasar lens**
SDSS J0757+2150	07:57:20.54	+21:50:07.7	MC	2.128	S, 2014 May (300B/L600)	720	Quasar+galaxy at $z = 0.118$
SDSS J0818+0601	08:18:30.46	+06:01:38.0	M	2.381	S, 2015 Feb (300B/L600)	900	Quasar pair $z = 2.359$&2.361
SDSS J0821+0735	08:21:43.36	+07:35:45.9	C	2.378	S, 2015 Feb (300B/L600)	1080	Quasar pair $z = 2.383$&2.387
SDSS J0821+4542	08:21:58.66	+45:42:44.4	M	2.066	S, 2014 May (300B/L600)	900	**Quasar lens** ($z_l = 0.349$)
SDSS J0826+4248	08:26:52.99	+42:48:17.8	MS	1.942	S, 2014 May (300B/L600)	900	Inconclusive
SDSS J0847+1504	08:47:21.96	+15:04:50.2	M	3.280	S, 2015 Feb (300B/SY47)	900	Different SED
SDSS J0921+2854	09:21:15.47	+28:54:44.3	MC	1.410	S, 2015 Feb (300B/L600)	720	**Quasar lens** ($z_l = 0.445^a$)
SDSS J0928+4332	09:28:39.19	+43:32:42.4	MC	3.698	S, 2014 May (300B/SY47)	900	Quasar pair $z = 3.694$&2.995
SDSS J0930+4614	09:30:21.16	+46:14:22.8	M	2.397	S, 2015 Feb (300B/L600)	900	Quasar pair $z = 2.393$&2.394
SDSS J0958+0744	09:58:42.24	+07:44:23.2	M	2.781	S, 2014 May (300B/L600)	900	Quasar+galaxy at $z = 0.158$
SDSS J1001+0156	10:01:40.95	+01:56:43.1	M	2.202	S, 2015 Feb (300B/L600)	1080	Different SED
SDSS J1043+4320	10:43:24.87	+43:20:49.4	M	2.234	S, 2015 Jun (300B/L600)	900	Quasar pair $z = 2.245$&2.225
SDSS J1108+4726	11:08:28.25	+47:26:21.6	C	3.627	S, 2014 May (300B/SY47)	900	Quasar+galaxy at $z = 0.385$
SDSS J1124+5710	11:24:55.24	+57:10:56.5	C	2.312	S, 2015 Feb (300B/L600)	720	Quasar pair $z = 2.309$&2.315
SDSS J1125+5020	11:25:42.60	+50:20:35.5	C	1.066	S, 2015 Jun (300B/L600)	900	Quasar+galaxy at $z = 0.385$
SDSS J1138+5254	11:38:38.54	+52:54:18.2	M	2.758	S, 2015 Jun (300B/L600)	1200	Different SED
SDSS J1139−0014	11:39:28.49	−00:14:18.1	C	3.084	S, 2014 May (300B/L600)	720	Quasar+star
SDSS J1152+2235	11:52:10.58	+22:35:19.2	C	2.902	S, 2014 May (300B/L600)	720	Quasar+star
SDSS J1248+6104	12:48:59.85	+61:04:30.3	C	2.591	S, 2015 Feb (300B/L600)	1200	Quasar+star
SDSS J1254+1857	12:54:40.37	+18:57:12.0	MC	1.717	S, 2015 Feb (300B/L600)	1200	**Quasar lens** ($z_l = 0.555^a$)
SDSS J1309+5617	13:09:27.55	+56:17:38.9	C	2.505	S, 2015 Jun (300B/L600)	1200	Quasar pair $z = 2.513$&2.515
SDSS J1319+5023	13:19:26.06	+50:23:05.5	C	2.301	S, 2015 Jun (300B/L600)	1080	Quasar+galaxy at $z = 0.088$
SDSS J1322+3038	13:22:04.81	+30:38:38.2	M	2.233	S, 2015 Jun (300B/L600)	1200	Inconclusive
SDSS J1330+3800	13:30:07.34	+38:00:42.4	C	2.254	S, 2015 Feb (300B/L600)	720	**Quasar lens**
SDSS J1405+1350	14:05:56.92	+13:50:38.3	C	2.342	S, 2015 Jun (300B/L600)	1200	Quasar pair $z = 2.345$&2.361
SDSS J1412+5204	14:12:10.18	+52:04:23.3	M	2.952	S, 2015 Feb (300B/L600)	1200	**Quasar lens**
SDSS J1429+2523	14:29:38.20	+25:23:43.4	M	3.904	S, 2015 Feb (300B/SY47)	900	Different SED
SDSS J1442+4055	14:42:54.79	+40:55:35.6	C	2.575	S, 2014 May (300B/L600)	480	**Quasar lens**
SDSS J1452+4224	14:52:11.50	+42:24:29.6	M	4.819	S, 2015 Feb (300B/SY47)	900	**Quasar lens** ($z_l = 0.382$)
SDSS J1458−0202	14:58:47.59	−02:02:05.9	M	1.724	S, 2014 May (300B/L600)	1200	**Quasar lens**
SDSS J1508+3037	15:08:22.32	+30:37:47.2	M	2.449	S, 2015 Feb (300B/L600)	1200	Inconclusive
SDSS J1537+3014	15:37:34.46	+30:14:53.7	MCS	1.553	S, 2014 May (300B/L600)	900	**Quasar lens** ($z_l = 0.490^a$)
SDSS J1548+2830	15:48:50.76	+28:30:14.3	C	3.227	S, 2015 Feb (300B/SY47)	900	Quasar pair $z = 3.208$&1.487
SDSS J1551+3303	15:51:37.02	+33:03:19.6	C	3.806	S, 2015 Feb (300B/SY47)	900	Different SED
SDSS J1552+2401	15:52:21.40	+24:01:23.1	MC	3.674	S, 2015 Feb (300B/SY47)	720	Quasar+star
SDSS J1554+2616	15:54:11.53	+26:16:35.7	C	2.321	S, 2015 Feb (300B/L600)	720	Quasar+star
SDSS J1556+1731	15:56:23.81	+17:31:21.4	C	2.814	S, 2014 May (300B/L600)	720	Quasar+galaxy at $z = 0.109$
SDSS J1600+3148	16:00:28.78	+31:48:31.7	C	2.331	S, 2015 Jun (300B/L600)	1080	Quasar+star
SDSS J1611+0844	16:11:05.64	+08:44:35.4	C	4.548	S, 2015 Feb (300B/SY47)	900	Different SED
SDSS J1627+5553	16:27:16.69	+55:53:37.0	C	4.072	S, 2015 Feb (300B/SY47)	720	Different SED
SDSS J1712+2516	17:12:32.14	+25:16:24.6	M	2.604	S, 2015 Feb (300B/L600)	1080	Quasar+star
SDSS J1715+2831	17:15:17.32	+28:31:29.5	C	2.023	S, 2015 Feb (300B/L600)	1080	Different SED
SDSS J2146-0047	21:46:46.03	−00:47:44.3	M	2.381	S, 2014 May (300B/L600)	900	**Quasar lens at $z = 0.799$**
SDSS J2220−0050	22:20:41.31	−00:50:15.5	MC	2.602	S, 2015 Jun (300B/L600)	1080	Quasar+star
SDSS J2238+1820	22:38:51.80	+18:20:38.5	MC	2.074	S, 2015 Jun (300B/L600)	720	Quasar+galaxy at $z = 0.199$
SDSS J2245+2548	22:45:55.75	+25:48:35.4	C	2.992	S, 2015 Jun (300B/L600)	900	Quasar pair $z = 2.995$&2.178
SDSS J2314−0108	23:14:24.50	−01:08:58.7	C	3.455	S, 2015 Feb (300B/SY47)	1080	Different SED

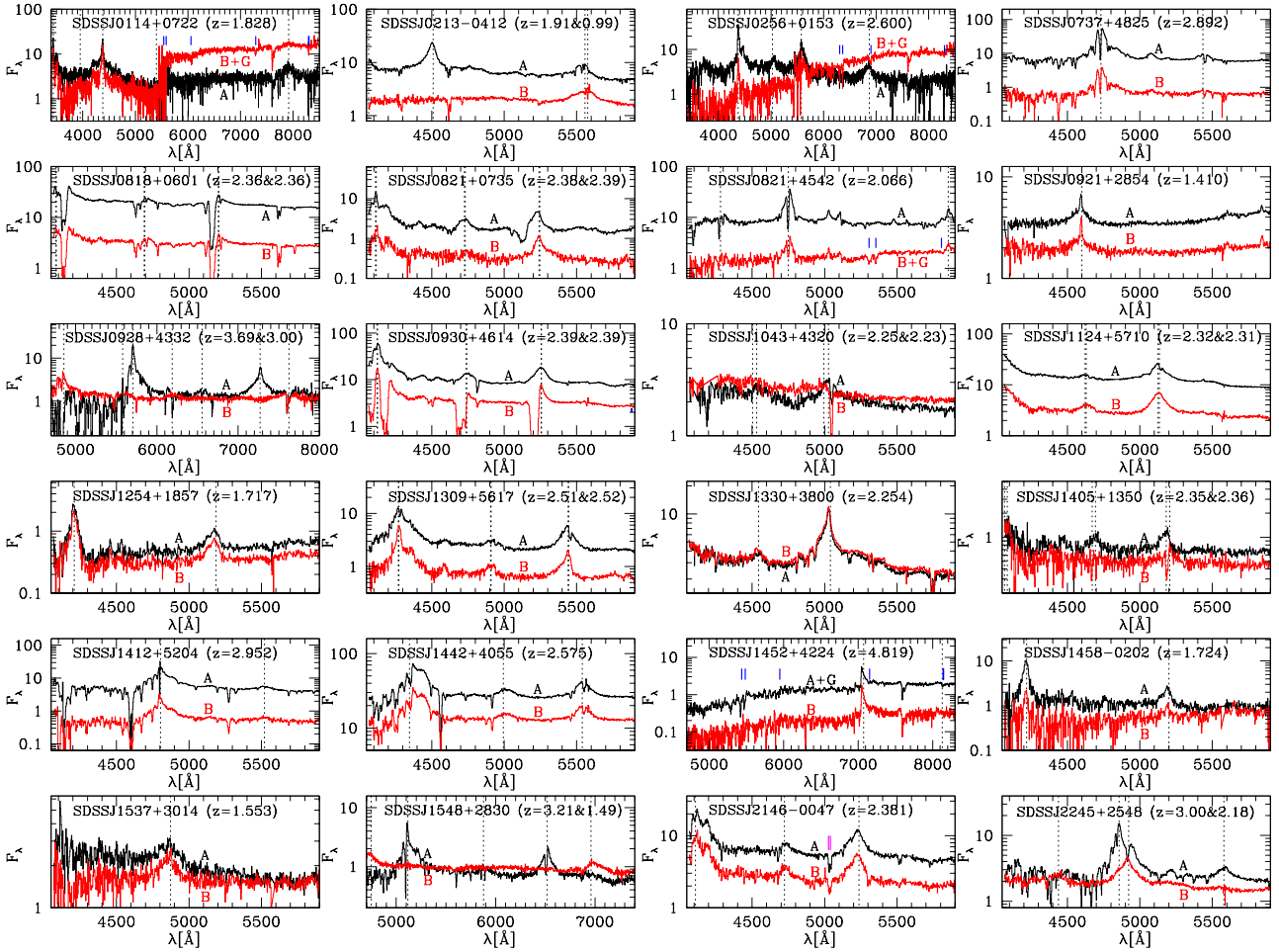

Figure 1. Spectra of the 24 confirmed quasar pairs, including 13 confirmed gravitationally lensed quasars (see Table 1). In each panel, vertical dotted lines show the wavelengths of the quasar emission lines. Vertical short bars indicate the wavelengths of absorption features in the spectrum of the lens galaxy, which are shown only for lens systems for which lens galaxies are sufficiently bright to be detected in one of the quasar spectra. The redshifts shown in each panel correspond to the quasar. The flux F_λ is in units of 10^{-17}erg cm^{-2} s^{-1} Å $^{-1}$.

13 systems are gravitationally lensed quasars. Our spectroscopy also identified an additional 11 quasar pairs with either almost identical or slightly different redshifts. Properties of these 11 quasar pairs will be discussed in Sections 3.3 and 5.3.

Fig. 1 presents the spectra for the 24 confirmed quasar pairs, including the 13 confirmed gravitationally lensed quasars. For five of the quasar lens systems, the lens galaxies are bright enough to be clearly detected in one of the quasar spectra. We successfully measured the lens redshift for these lens systems (see Table 1). For an additional three quasar systems, the lens galaxies are bright and their redshifts were derived from the SDSS-III spectra. The subsequent spectra do not cover the red wavelength range where these lens galaxies can be detected easily.

3.2 Imaging

We imaged a subsample of the most promising candidates in two to three bands with the goal of detecting the lens galaxy. At minimum, these imaging data should better resolve the small separation lensed quasar images to provide the basic constraints required for mass modelling. The majority of the lenses from the BQLS sample were observed with the Tektronix 2048×2048 CCD camera (Tek2k, with a pixel resolution of 0.22 arcsec) on the UH88 telescope. A few of the candidates were observed with other telescopes. A summary of these observations is given in Table 2 which includes the exposure times for each filter. We used the FOCAS instrument with 2 × 2 binning on Subaru giving a pixel resolution of 0.208 arcsec, the

Table 2. Summary of imaging observations of the confirmed lenses.

Object ID	Instrument	Observing date	Exposure (s)
J0114+0722	Tek2k	2013 Dec 24	1440 (*V*,*I*)
J0256+0153	Tek2k	2013 Dec 24	1440 (*V*,*I*)
J0737+4825	Tek2k	2015 Feb 20	1440 (*V*,*I*)
J0821+4542	Tek2k	2014 Feb 21	2160 (*V*) 1980 (*R*)
J0921+2854	Tek2k	2015 Feb 20	1440 (*V*) 1080 (*I*)
J1254+1857	Tek2k	2014 Feb 21	3060 (*V*) 2880 (*R*)
J1330+3800	Tek2k	2014 Feb 21	1440 (*V*) 2160 (*R*)
J1412+5204	Tek2k	2015 Feb 20	1440 (*V*,*I*)
J1442+4055	OSMOS	2013 Apr 08	1200 (*g*) 2100 (*r*) 900 (*i*,*z*)
J1452+4224	FOCAS	2015 Jun 19	270 (*R*) 360 (*I*)
J1458−0202	SOI	2013 Feb 12	420 (*g*,*r*,*i*)
J1537+3014	Tek2k	2014 Feb 21	1440 (*V*) 1800 (*R*)
J2146−0047	Tek2k	2012 Sep 17	960 (*V*,*I*)

Note. Tek2k is on the UH88 telescope, OSMOS is on the Hiltner telescope, FOCAS is on the Subaru telescope and SOI is at the SOAR telescope.

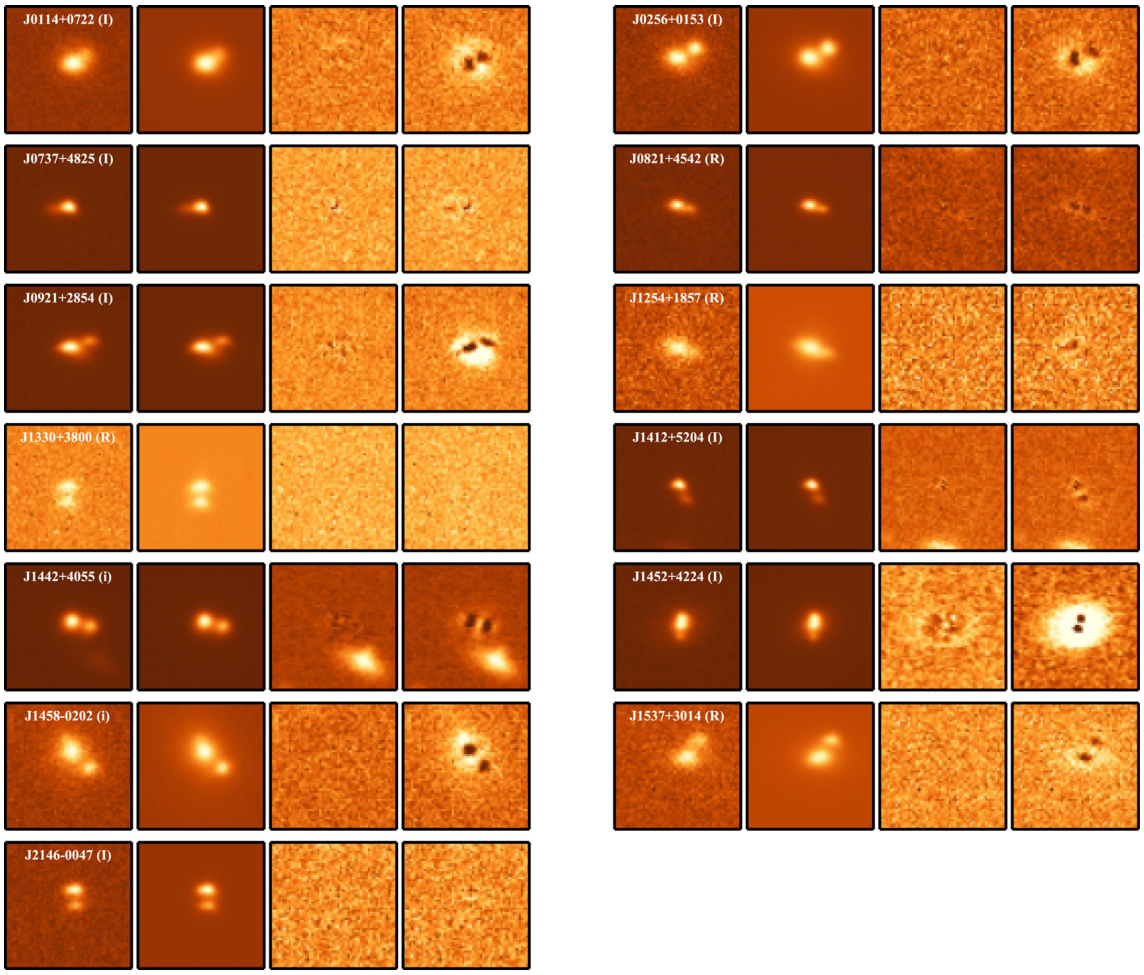

Figure 2. GALFIT modelling results for the quasar lens sample using the reddest available band as labelled in each case. For each lens system, the columns from left to right are the data, the GALFIT model including the lens galaxy and the residuals with and without the lens galaxy, respectively. The flux scales in the data and model images match but they are different from the residual images. The flux scales of both residual images match. All images have the standard orientation with north up and east on the left. All images are 51 pixels on the side, which is ∼11 arcsec for all systems except for J1442+4055 (∼14 arcsec) and J1458−0202 (∼8 arcsec).

SOI instrument (pixel resolution of 0.15 arcsec) on the SOuthern Astrophysical Research (SOAR) telescope and the OSMOS instrument (pixel resolution of 0.273 arcsec) on the Hiltner telescope of the MDM observatory. We processed the data in IRAF by following standard procedures. The seeing of our imaging data is better than 1 arcsec.

In most cases, the imaging reveals two point-like components with a hint of extended emission close to one of those components indicating presence of a lens galaxy. We use GALFIT (Peng et al. 2002, 2010) to model each of these components and to measure their fluxes and positions. The quasars are assumed to be point sources convolved with the PSF and the galaxy is modelled with a Sérsic profile. The use of point sources for the quasar components is reasonable because all the quasars are at high redshifts $z > 1$. We use the nearby stars as a model for the PSF. We first fit models to the two quasars without the lens. Next, we fit models including the lens. Both modelling results are compared and the latter model is accepted if the χ^2 and the residuals have improved. In the cases when it was difficult to fit the Sérsic index of the galaxy's light profile, we held it fixed at $n = 4$, since the de Vaucouleurs profile (de Vaucouleurs 1948) is a good model for early-type galaxies. The modelling results for all of the 13 confirmed lenses are presented in Fig. 2. For each lens, we show the reddest available image (left-hand panel) where the contribution from the lens galaxy is easier to see than in the other bands, the GALFIT model which includes the lens galaxy (second panel from left) and the residuals from this model (third panel from left). For comparison, we also show the residuals from the model without the lens galaxy in the right-most panel.

We performed relative photometry of the lenses by comparing them to nearby stars with known SDSS magnitudes. First, we used the software from Astrometry.net (Lang et al. 2010) to determine the orientations of the images and the positions of the stars, except for SDSS J1458−0202 and SDSS J1452+4224 where the astrometry was determined manually. For every lens in every band available from the imaging, we measured the fluxes of about a dozen stars using SEXTRACTOR (Bertin & Arnouts 1996). The zero-points were determined by comparing the SDSS magnitudes to the fluxes of the stars. Owing to the differences between the SDSS filters and those used for the follow up observations, we had to apply appropriate filter conversions to the fluxes. We adopted the conversions from Jester et al. (2005) and Lupton (2005, unpublished) which are available at https://www.sdss3.org/dr8/algorithms/sdssUBVRITransform.php. The zero-points were then used for determining the magnitudes of the lensed quasars and lens

Table 3. Relative astrometry and photometry of the 13 confirmed lens systems.

Object ID and filters	Component	RA (J2000)	Dec. (J2000)	Red (I, i or R)	Blue (V, g or$R$)
SDSS J0114+0722	A	01:14:38.421	+07:22:28.50	20.88 ± 0.07	22.70 ± 0.17
I,*V*	B	01:14:38.322	+07:22:29.35	21.20 ± 0.03	22.98 ± 0.09
	G	01:14:38.386	+07:22:28.60	19.30 ± 0.03	20.56 ± 0.03
SDSS J0256+0153	A	02:56:40.771	+01:53:29.28	21.20 ± 0.05	22.60 ± 0.09
I,*V*	B	02:56:40.653	+01:53:30.06	20.79 ± 0.01	22.33 ± 0.04
	G	02:56:40.740	+01:53:29.12	19.89 ± 0.04	20.50 ± 0.89
SDSS J0737+4825	A	07:37:08.677	+48:25:51.45	18.28 ± 0.00	19.26 ± 0.00
I,*V*	B	07:37:08.829	+48:25:51.26	20.58 ± 0.07	22.03 ± 0.14
	G	07:37:08.782	+48:25:51.32	19.87 ± 0.10	22.11 ± 0.15
SDSS J0821+4542	A	08:21:58.706	+45:42:44.40	20.76 ± 0.14	20.01 ± 0.02
R,*V*	B	08:21:58.582	+45:42:44.07	20.86 ± 0.02	21.54 ± 0.07
	G	08:21:58.678	+45:42:44.38	20.01 ± 0.06	–
SDSS J0921+2854	A	09:21:15.494	+28:54:44.57	18.03 ± 0.01	20.36 ± 0.01
I,*V*	B	09:21:15.355	+28:54:45.10	18.93 ± 0.01	20.93 ± 0.01
	G	09:21:15.433	+28:54:44.35	18.28 ± 0.01	20.28 ± 0.08
SDSS J1254+1857	A	12:54:40.445	+18:57:12.33	21.98 ± 0.18	–
R	B	12:54:40.295	+18:57:11.44	21.74 ± 0.07	–
	G	12:54:40.385	+18:57:11.89	20.02 ± 0.11	–
SDSS J1330+3800	A	13:30:07.330	+38:00:43.82	20.16 ± 0.11	19.52 ± 0.02
R,*V*	B	13:30:07.343	+38:00:42.39	20.03 ± 0.04	19.69 ± 0.02
	G	13:30:07.375	+38:00:43.64	19.74 ± 0.15	–
SDSS J1412+5204	A	14:12:10.158	+52:04:23.50	18.91 ± 0.01	19.85 ± 0.00
I,*V*	B	14:12:10.080	+52:04:22.16	20.98 ± 0.09	22.00 ± 0.02
	G	14:12:10.114	+52:04:22.46	20.16 ± 0.06	–
SDSS J1442+4055	A	14:42:54.795	+40:55:35.74	17.64 ± 0.00	18.14 ± 0.00
i,*g*	B	14:42:54.614	+40:55:35.18	18.28 ± 0.01	18.83 ± 0.00
	G	14:42:54.696	+40:55:35.38	18.83 ± 0.05	20.07 ± 0.10
SDSS J1452+4224	A	14:52:11.500	+42:24:29.02	20.08 ± 0.02	21.05 ± 0.02
I,*R*	B	14:52:11.490	+42:24:30.61	20.91 ± 0.02	21.71 ± 0.02
	G	14:52:11.490	+42:24:29.62	18.15 ± 0.02	18.68 ± 0.06
SDSS J1458−0202	A	14:58:47.580	−02:02:05.16	21.50 ± 0.02	24.50 ± 0.10
i,*g*	B	14:58:47.670	−02:02:03.49	23.16 ± 0.15	22.76 ± 0.02
	G	14:58:47.650	−02:02:04.19	18.96 ± 0.07	21.51 ± 0.08
SDSS J1537+3014	A	15:37:34.484	+30:14:53.70	22.02 ± 0.15	21.95 ± 0.10
R,*V*	B	15:37:34.375	+30:14:55.49	21.14 ± 0.03	21.97 ± 0.18
	G	15:37:34.442	+30:14:54.12	18.95 ± 0.29	20.84 ± 0.06
SDSS J2146−0047	A	21:46:46.025	−00:47:44.10	19.74 ± 0.02	20.29 ± 0.04
I,*V*	B	21:46:46.018	−00:47:45.48	20.54 ± 0.05	21.57 ± 0.19
	G	21:46:46.020	−00:47:44.82	21.37 ± 0.32	21.29 ± 0.31

galaxies. The results of the relative astrometry and photometry are given in Table 3. The best-fitting parameters of the Sérsic model assumed for the lens galaxies are reported in Table 4.

3.3 Notes on interesting individual systems

Here, we discuss the properties of some of the interesting systems from the BQLS.

3.3.1 SDSS J0818+0601

The spectrum shown in Fig. 1 indicates that the two stellar components separated by $\Delta\theta \sim 1$ arcsec have similar spectra ($\Delta V = 226\,\mathrm{km\,s^{-1}}$), including broad absorption features in the Ly α and C IV emission lines. However, no lens galaxy was found in our SOAR images (420 s in *i*). If this is a gravitational lens, the non-detection of the lens suggests it is at a relatively high redshift ($z_l \gtrsim 1$).

3.3.2 SDSS J0821+0735

While the spectra of the components (Fig. 1) indicate that the quasar redshifts are almost same ($\Delta V = 319\,\mathrm{km\,s^{-1}}$), their SEDs appear to be slightly different. The emission line features have different profiles and the continuum shows differences in the slope. Some differences in the SEDs of lensed counterparts can be attributed to dust extinction in the lens galaxy (e.g. Falco et al. 1999) or microlensing. However, the UH88 imaging observation (1440 s in *I*) also failed to detect any lens between the quasar components.

3.3.3 SDSS J0921+2854

After we confirmed the lensing nature of this object, an archival search revealed that this lens was independently discovered by E. Ofek et al., and was observed by the *Hubble Space Telescope* Cycle 20 programme GO-13001 although their results are unpublished.

Table 4. Sérsic parameters of the lens galaxies. The parameters r_e, n, e, and θ_e denote the effective radius, Sérsic index, ellipticity, and the position angle (measured counter-clockwise from north where north is up at 0°), respectively. See Table 3 for the magnitudes.

Object ID	r_e (arcsec)	n	e	θ_e (°)
J0114+0722	0.84 ± 0.04	2.13 ± 0.24	0.23 ± 0.02	73.3 ± 6.2
J0256+0153	1.16 ± 0.06	1.35 ± 0.21	0.33 ± 0.03	72.5 ± 4.3
J0737+4825	1.08 ± 0.35	[4.00]	0.14 ± 0.12	−70.0 ± 32.6
J0821+4542	0.14 ± 0.02	[4.00]	[0.00]	[0.0]
J0921+2854	0.70 ± 0.01	0.98 ± 0.06	0.10 ± 0.02	36.7 ± 9.6
J1254+1857	0.73 ± 0.14	[4.00]	0.38 ± 0.12	−16.1 ± 14.5
J1330+3800	0.87 ± 0.34	[4.00]	0.75 ± 0.16	−16.3 ± 9.7
J1412+5204	0.61 ± 0.15	[4.00]	0.58 ± 0.08	15.5 ± 7.4
J1442+4055	0.99 ± 0.10	4.19 ± 0.70	0.21 ± 0.03	68.2 ± 6.1
J1452+4224	1.09 ± 0.01	[4.00]	0.30 ± 0.01	−23.8 ± 1.1
J1458−0202	2.13 ± 0.24	3.81 ± 0.30	0.36 ± 0.02	30.6 ± 1.6
J1537+3014	3.57 ± 2.09	5.90 ± 1.92	0.37 ± 0.04	87.2 ± 5.1
J2146−0047	0.38 ± 0.28	[4.00]	[0.00]	[0.0]

There are also X-ray and radio detections for this system, probably emanating from the lensed quasar.

3.3.4 SDSS J0930+4614

This is a quasar pair at the same redshift ($\Delta V = 111$ km s^{-1}) but with quite different SEDs (Fig. 1). The fainter component has broad absorption lines associated with Ly α, Si IV, and C IV emission lines, while the brighter component has no broad absorption features. Given the markedly different SEDs, this is likely to be a physical quasar pair rather than a lens.

3.3.5 SDSS J1043+4320

This is a quasar pair with similar redshifts ($\Delta V = 1778$ km s^{-1}). There are strong absorption lines in the C IV emission lines of both components, but the overall SED shapes appear to be different (see Fig. 1). It is important to conduct a deep imaging to search for a possible lens galaxy.

3.3.6 SDSS J1124+5710

The SEDs of this quasar pair appear similar but have slightly different redshifts ($\Delta V = 496$ km s^{-1}, Fig. 1). There is no indication of a lens galaxy in our UH88 imaging (1440 s in *I*). Hence, we conclude that this is likely a binary quasar system.

3.3.7 SDSS J1309+5617

While the redshifts of the two components are almost identical ($\Delta V = 169$ km s^{-1}), the significantly different shapes of the Ly α and C IV emission lines mean that this system is likely to be a binary quasar system rather than a lens.

3.3.8 SDSS J1405+1350

The SED of the fainter quasar has some similarity with the SED of the brighter quasar but the emission features have very low signal-to-noise ratios. The redshifts are not identical but imply that the quasars are probably physically associated ($\Delta V = 1400$ km s^{-1}). Additionally, the non-detection of a putative lens galaxy suggests this might be a binary quasar system.

3.3.9 SDSS J1452+4224

At $z_s \approx 4.8$,[2] the quasar redshift of this lens is one of the highest redshifts known and is comparable to the lens SDSS J0946+1835 (McGreer et al. 2010). The total lensing magnification is predicted to be ∼8 by our mass models in Section 4. The lens galaxy is quite visible in the spectrum and the image, and has one of the lowest measured lens redshift ($z_l = 0.382$) in our sample. Coincidentally, the lens galaxy of SDSS J0946+1835 is at a similar redshift but more massive given the wider image separations of the lensed quasars.

3.3.10 SDSS J2146−0047

While the lensing nature of this object was confirmed by our imaging and spectroscopic follow-up observations, Agnello et al. (2015b) recently reported an independent discovery of this lens using Dark Energy Survey data. They tentatively assigned a lens redshift of $z_l = 0.799$ based on Mg II and Fe II absorption features in the quasar spectra. The absorption feature is also seen in the Subaru spectrum shown in Fig. 1.

4 MASS MODELLING

We created mass models for the 13 spectroscopically confirmed lens systems with the modelling software, GLAFIC (Oguri 2010). The redshifts of the quasars and the lens galaxies were taken from Table 1. For those systems with no lens redshifts, we adopted a fiducial value of $z_l = 0.5$ (∼peak of the redshift distribution of typical lenses e.g. see Fig 3), as a lens redshift is required in the estimate of the velocity dispersion.

We assumed that the mass distribution of the lens galaxies is isothermal. More specifically, we either used the singular isothermal sphere (SIS) or ellipsoid (SIE) model for the lenses. Parameters such as the mass, ellipticity and the position angle (θ_e) of the lens model and the true (unlensed) position of the lensed quasar are allowed to be free. The positions and flux ratios[3] of the lensed quasar images served as constraints. We always begin with the SIS model and add further complexity such as adding more parameters only if the SIS results in a poor fit. The best-fitting parameters from the mass models are reported in Table 5.

For SDSS J1330+3800, neither the SIS nor the SIE model could fit the constraints well. Hence, for this system, we used an SIS model with the lens galaxy position allowed to vary within the uncertainties from the GALFIT model. In a few other cases, we also used priors on the position angle of the lens based on the photometric models (see Table 5). In general, we could use the GALFIT errors on the positions and fluxes of the lensed images but had to relax them[4] in a few cases in order to find a reasonable χ^2. The errors were relaxed up

[2] Redshifts from Ly α at such high redshifts are strongly affected by the Ly α forest (McGreer et al. 2010). Therefore, we give fewer significant digits on the redshift estimate.

[3] The flux ratios are often known to be affected by dust, substructure, intrinsic quasar variability and microlensing. Thus, a simple globally smooth models such as the ones tested here may fail to fit the flux ratios and cannot necessarily be used to rule out the lens hypothesis.

[4] This is reasonable because the errors from GALFIT are known to be an underestimate (e.g. Rusu et al. 2015).

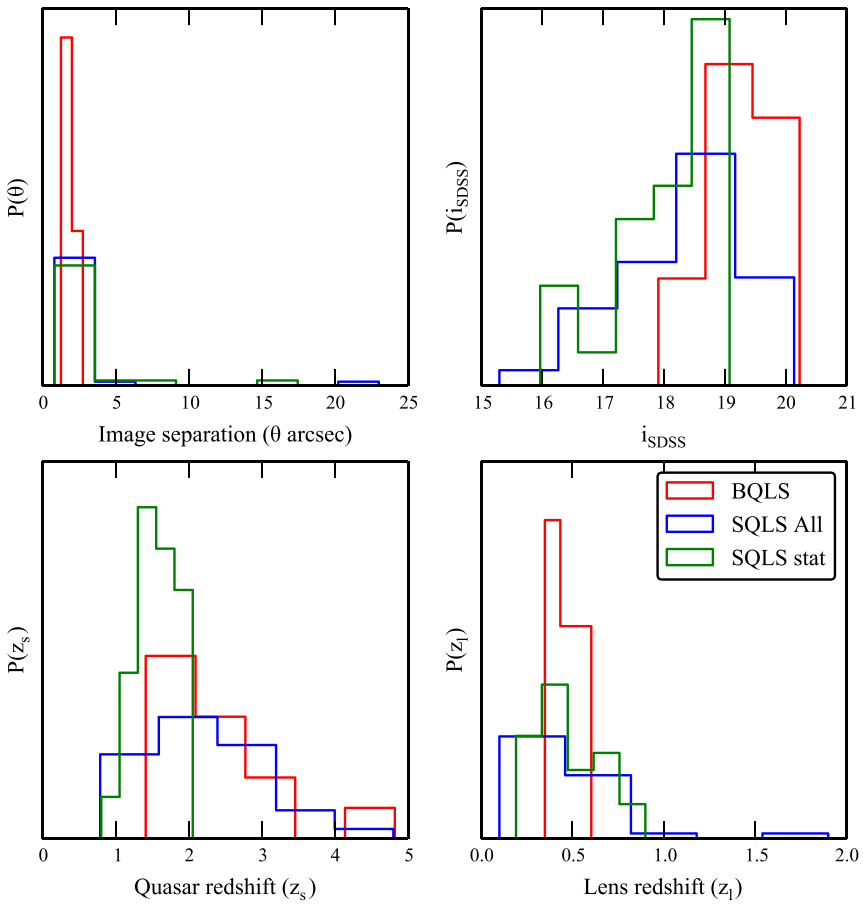

Figure 3. Comparison of the BQLS with the SQLS 'statistical' and 'all' samples. Owing to the smaller sample size of BQLS, a qualitative comparison is more meaningful. Each histogram is thus normalized and integrates to unity. Lenses with no known lens redshifts are excluded from the panel showing the redshift distributions. BQLS lenses are fainter and have smaller image separations. The quasar redshift distribution and the peak of the lens redshift distribution of the BQLS sample are similar to the SQLS 'all' sample.

Table 5. Best-fitting lens mass model parameters. The parameter $\theta_{\rm Ein}$, e, and $\theta_{\rm e}$ denote the Einstein radius, ellipticity, and the position angle of the mass distribution, respectively. The numbers in bracket indicate which priors were used from the GALFIT model (see Table 3).

Object ID	$\theta_{\rm Ein}$ (arcsec)	e	$\theta_{\rm e}$ (°)
SDSS J0114+0722	0.83	0.42	45
SDSS J0256+0153	1.03	0.74	42
SDSS J0737+4825	0.81	0.25	[−82]
SDSS J0821+4542	0.63	0.51	−21
SDSS J0921+2854	0.96	0.53	28
SDSS J1254+1857	1.15	–	–
SDSS J1330+3800	0.89	[−0.553]	[0.321][a]
SDSS J1412+5204	0.84	0.45	52
SDSS J1442+4055	1.03	–	–
SDSS J1452+4224	0.87	–	–
SDSS J1458−0202	1.15	0.27	14
SDSS J1537+3014	1.14	0.21	[88]
SDSS J2146−0047	0.71	–	–

Note. [a]This is an SIS model with priors on the lens position. Instead of the ellipticity and position angle, the last two columns list the best-fitting offset (in arcseconds) of the lens from one of the lensed quasars in x and y direction, respectively. We use the standard Cartesian convention where x and y are positive to the right and up, respectively.

to ∼0.15 arcsec and were always smaller than the pixel size. The best-fitting Einstein radii (or the velocity dispersions) of the BQLS lenses, which is a proxy for the mass of the lens galaxy, are similar to typical galaxy-scale lenses (e.g. Bolton et al. 2006a).

5 DISCUSSION

5.1 Properties of the BQLS

The basic properties of the 13 quasar lenses are summarized in Table 6. We also compare the image separation, magnitude, and redshift distributions of the newly discovered quasar lens systems with those of the SQLS sample in Fig. 3. In the redshift comparison, we exclude systems for which the lens redshifts are not known. There are two SQLS lens samples (Inada et al. 2012): (i) 'all' – the entire lens sample which includes some heterogeneously selected lenses and (ii) 'stat' – this is a statistically well-defined sample with high completeness. The SQLS statistical lens sample is limited to the quasar redshift range of $0.6 < z < 2.2$, i-band magnitude $i < 19.1$, image separations 1 arcsec $< \Delta\theta <$ 30 arcsec, and flux ratios for doubles larger than $10^{-0.5}$, in order to accurately characterize the selection function.

Since the BOSS sample size is much smaller, we show normalized distributions to facilitate qualitative comparison of the

Table 6. Summary of the confirmed quasar lenses. The image separations $\Delta\theta$ are computed from Table 3 and the *i*-band PSF magnitudes are from the SDSS data base.

Object ID	z_s	z_l	$\Delta\theta$(arcsec)	i
SDSS J0114+0722	1.828	0.408	1.70	19.1
SDSS J0256+0153	2.600	0.603	1.93	20.0
SDSS J0737+4825	2.892	–	1.54	18.5
SDSS J0821+4542	2.066	0.349	1.35	18.9
SDSS J0921+2854	1.410	0.445	1.91	18.9
SDSS J1254+1857	1.717	0.555	2.32	19.5
SDSS J1330+3800	2.254	–	1.44	20.1
SDSS J1412+5204	2.952	–	1.53	19.0
SDSS J1442+4055	2.575	–	2.13	17.9
SDSS J1452+4224	4.819	0.382	1.59	19.1
SDSS J1458−0202	1.724	–	2.15	19.1
SDSS J1537+3014	1.553	0.490	2.30	19.6
SDSS J2146−0047	2.381	0.799	1.39	20.2

properties of these samples. The image separation distribution suggests that the BOSS sample finds a larger fraction of small image separation ($\Delta\theta \lesssim 2$ arcsec) lenses compared to the SQLS sample. One likely reason for this difference is that we preferentially selected small-separation lens candidates for follow-up confirmation because larger separation quasar pairs are more likely to be physical pairs rather than real lenses (e.g. Kochanek, Falco & Muñoz 1999; Hennawi et al. 2006a). Another possibility may be fibre collisions. Large-separation lenses are produced by clusters of galaxies typically at $z \sim 0.5$, and therefore there are usually many member galaxies around the quasar images that are selected as Constant MASS (CMASS) galaxies for spectroscopy. This may reduce the chance of these quasar images being spectroscopically observed by BOSS. As mentioned earlier, this was indeed the case for SDSS J2222+2745 where none of the quasar images were observed by BOSS while spectra were taken of several nearby member galaxies of this cluster lens.

We find that 7 out of the 13 confirmed quasar lens systems are located at $z > 2.2$. The fraction of high-redshift quasar lenses is not particularly high compared with the 'all' SQLS sample (see Fig. 3). This result may be partly explained by the fact that some of the new lens systems were originally targeted as CMASS galaxies rather than quasars because of the dominant lens galaxy component. Indeed, for many of these cases, the lens galaxies are visible in the SDSS spectra which then provide the lens redshifts for these systems (see Table 1). Spectroscopic quasars selected in this manner are not necessarily high-redshift quasars. This also explains the peak of the lens redshift distribution at $z_l \sim 0.5$, which is close to the median redshift of the BOSS CMASS galaxy sample.

Most of the BQLS lenses are fainter because BOSS target selection selects fainter quasars. The BOSS DR12 quasar catalogue contains 25 previously known lenses, many found by the SQLS. About two-thirds of this sample are bright lens systems ($i < 18$) with quasars at low redshifts ($z < 2.2$). We excluded this known sample before the visual selection of the BQLS lens candidates.

A subsample of the BOSS quasars are selected homogeneously and have a well-defined selection function which is called the CORE sample (Ross et al. 2012). Lenses present in the CORE sample could be used to define a statistical sample for the BQLS provided the visual selection process is calibrated. However, only two out of the 13 confirmed lenses are in the CORE sample (using the boss_target1 flag for QSO_CORE_MAIN). It is unlikely that our visual inspection process is highly inefficient, so it is unlikely that we are missing a large number of true lenses. Therefore, even if we were to detect most of the true lenses, a statistically well-defined sample derived from this parent sample will still be probably too small for any statistical study. The 'point-source' requirement for the CORE sample is probably the cause of this low yield.

5.2 Quad fraction

All of the 13 confirmed quasar lenses are two-image quasar lens systems. At galaxy scales, we expect about 15–20 per cent of the lenses to be quadruply imaged for the BOSS quasar lens sample with $i \lesssim 20-21$ (Oguri & Marshall 2010) which means we should expect two or more quad lenses in our sample. There are several possible explanations for the lack of quad lenses in the BOSS quasar lens sample. First of all, the BOSS quasar target selection selects only point sources to increase its efficiency (Ross et al. 2012), whereas small-separation quad lens systems are often classified as extended sources in the SDSS (Oguri et al. 2006). Indeed, all the four small-separation ($\Delta\theta < 2$ arcsec) quad lenses discovered in the SQLS (see Inada et al. 2012) are found to be classified as extended sources in the SDSS data set. In addition, the visual inspection method might be biased against selecting quad lenses because the quads appear to have odd morphology. And, spectroscopic follow-up observations might be biased because single long-slit mode is used to target the double quasar candidate images along with the candidate lens galaxy for confirmation. Therefore, it is of great interest to apply more sophisticated algorithms (e.g. Agnello et al. 2015a; Chan et al. 2015) to the quasars in BOSS to search for quad lenses that are missing in the current lens sample.

5.3 Quasar pairs

Our follow-up spectroscopy identified an additional 11 quasar pairs with small angular separations of $\Delta\theta < 3$ arcsec (see Table 7 for a summary). We expect most of these to be either projected pairs or binary quasars, based on their different SEDs and the lack of an obvious lens. Among the 11 quasar pairs, 7 pairs have the velocity difference ΔV smaller than 2000 km s^{-1} and therefore satisfy the criterion of physical binaries used in Hennawi et al. (2006a). The velocity difference may also be useful for distinguishing binary quasars from lensed quasars. We find that the typical ΔV of the confirmed lenses measured from our follow-up spectra is <40 and ∼100 km s^{-1} in a few cases, which can be regarded as a typical error on our velocity difference measurements. From Table 7, we find that most of the quasar pairs have velocity differences significantly larger than those of the confirmed lenses, indicating that they are less likely to be lensed images of a single source but rather are physically associated distinct quasars.

In general, there are still only a small number of quasar pairs known (Hennawi et al. 2006b, 2010; Myers et al. 2008; Kayo & Oguri 2012), and our sample adds significantly to the existing pair samples. For comparison, the SQLS only identified eight binary quasars with $\Delta\theta < 3$ arcsec (see Kayo & Oguri 2012, for a compilation), which is comparable to the number of new binary quasars from the BQLS. The small-separation binary quasars have been used to study the very small scale clustering of quasars to discuss the possible role of mergers in enhancing quasar activities (Hennawi et al. 2006b; Hopkins et al. 2008; Myers et al. 2008; Shen et al. 2010; Kayo & Oguri 2012). Projected quasar pairs are also useful for studying the distribution of absorbers around quasars (Hennawi et al. 2006a).

Table 7. Summary of confirmed quasar pairs. See Table 1 for the RA and Dec. of the brighter quasar image (A). The positions and the *i*-band magnitudes in this table are from the SDSS data base except for J0818+0601 where we used the astrometrically calibrated SOAR images.

Object ID	RA_B	$Dec._B$	z_A	z_B	$\Delta\theta$(arcsec)	i_A	i_B	Δ V (km s^{-1})
SDSS J0213−0421	02:13:22.865	−04:21:34.341	1.911	0.992	2.0	20.8	18.8	>2000
SDSS J0818+0601	08:18:30.420	+06:01:37.860	2.359	2.361	1.1	18.1	20.0	226
SDSS J0821+0735	08:21:43.241	+07:35:45.108	2.383	2.387	1.3	20.7	21.6	319
SDSS J0928+4332	09:28:39.048	+43:32:42.141	3.694	2.995	1.6	21.1	20.3	>2000
SDSS J0930+4614	09:30:20.986	+46:14:23.260	2.393	2.394	1.5	18.4	19.9	111
SDSS J1043+4320	10:43:25.025	+43:20:48.958	2.245	2.225	1.7	21.4	20.7	1778
SDSS J1124+5710	11:24:55.440	+57:10:58.120	2.309	2.315	2.0	18.6	19.7	496
SDSS J1309+5617	13:09:27.338	+56:17:41.161	2.513	2.515	2.8	20.5	21.6	169
SDSS J1405+1350	14:05:56.865	+13:50:39.827	2.345	2.361	1.7	21.7	22.0	1400
SDSS J1548+2830	15:48:50.776	+28:30:12.714	3.208	1.487	1.7	20.8	20.9	>2000
SDSS J2245+2548	22:45:55.801	+25:48:33.548	2.995	2.178	2.0	20.4	20.7	>2000

6 SUMMARY AND CONCLUSION

We present the initial results from BQLS, a systematic search for lensed quasars in the SDSS-III/BOSS data. We applied the same technique that we used for finding lensed quasars in the SDSS DR7 (SQLS). Here, we report the discovery of 13 confirmed quasar lenses. In addition, we present the discovery of 11 quasar pairs, some of which may consist of physical binaries. This subsample may still contain a few unrecognized lenses. The sample of new lenses includes one of the highest redshift lensed quasar (SDSS J1452+4224, $z \approx 4.8$) found to date. SDSS J1442+4055 was also discovered independently by Sergeyev et al. 2015 (submitted to MNRAS, private communication from Luis J. Goicoechea). All the confirmed lenses from the BQLS have only two images. The lack of quad lenses is probably because BOSS only selects point-like quasars. We note that our follow-up observations are still incomplete with an additional ∼50 good lens candidates that need verification. However, this sample is likely to have fewer real lenses since we conducted the follow-up observations of the most promising candidates first.

Compared to the SQLS, the selection function of the BQLS sample is complicated owing to the complex selection of the initial BOSS quasar targets. In addition to the incomplete follow-up observations, a complex selection function prevents us from using the BQLS sample for statistical studies of either the lens population or cosmology (e.g. Oguri et al. 2012). The CORE sample from BOSS, which is a uniform and well-defined quasar sample could be used to produce a statistical BQLS sample, yielded only two lenses. This is probably because the quasars are required to be point-like in the CORE sample.

A qualitative comparison of the initial BQLS sample with the SQLS shows that BQLS lenses are somewhat fainter and have smaller image separations, presumably due to the BOSS selection criteria. Furthermore, the BQLS and SQLS lensed quasars have similar redshift distributions in spite of the higher redshift selection used for BOSS quasars. This is because many of the lenses in our sample were photometrically identified as galaxies before they were spectroscopically confirmed by BOSS to be quasars. In addition, about half of the lensed quasars have redshifts lower than the quasar redshift range targeted by BOSS. These lenses would have been missed in the absence of BOSS CMASS galaxy spectroscopy.

This study provides useful guidance for ongoing quasar lens surveys in Hyper Suprime-Cam[5] and Dark Energy Survey (The Dark Energy Survey Collaboration 2005) in which even fainter quasar lenses will be discovered.

[5] http://www.naoj.org/Projects/HSC/surveyplan.html

ACKNOWLEDGEMENTS

The work of MO and AM was supported in part by World Premier International Research Center Initiative (WPI Initiative), MEXT, Japan. This work was also supported by Grant-in-Aid for Scientific Research from the JSPS (26800093 and 24740171). AM would like to thank S. More and J. Silverman for useful suggestions. AM acknowledges the support of the Japan Society for Promotion of Science (JSPS) fellowship. AMM acknowledges the support of NSF grant AST-1211146. The authors would like to thank the anonymous referee for useful suggestions that improved the paper.

Funding for SDSS-III has been provided by the Alfred P. Sloan Foundation, the Participating Institutions, the National Science Foundation, and the US Department of Energy Office of Science. The SDSS-III web site is http://www.sdss3.org/. SDSS-III is managed by the Astrophysical Research Consortium for the Participating Institutions of the SDSS-III Collaboration including the University of Arizona, the Brazilian Participation Group, Brookhaven National Laboratory, Carnegie Mellon University, University of Florida, the French Participation Group, the German Participation Group, Harvard University, the Instituto de Astrofisica de Canarias, the Michigan State/Notre Dame/JINA Participation Group, Johns Hopkins University, Lawrence Berkeley National Laboratory, Max Planck Institute for Astrophysics, Max Planck Institute for Extraterrestrial Physics, New Mexico State University, New York University, Ohio State University, Pennsylvania State University, University of Portsmouth, Princeton University, the Spanish Participation Group, University of Tokyo, University of Utah, Vanderbilt University, University of Virginia, University of Washington, and Yale University.

Based in part on data collected at Subaru Telescope, which is operated by the National Astronomical Observatory of Japan. Use of the UH 2.2-m telescope for the observations is supported by NAOJ. Some of the data presented herein were obtained at the W.M. Keck Observatory, which is operated as a scientific partnership among the California Institute of Technology, the University of California and the National Aeronautics and Space Administration. The Observatory was made possible by the generous financial support of the W.M. Keck Foundation. The authors wish to recognize and acknowledge the very significant cultural role and reverence that the summit of Mauna Kea has always had within the indigenous Hawaiian community. We are most fortunate to have the opportunity to

conduct observations from this mountain. A part of this work is based on observations obtained at the MDM Observatory, operated by Dartmouth College, Columbia University, Ohio State University, Ohio University, and the University of Michigan. Based on observations obtained at the SOAR telescope, which is a joint project of the Ministério da Ciência, Tecnologia, e Inovação (MCTI) da República Federativa do Brasil, the US National Optical Astronomy Observatory (NOAO), the University of North Carolina at Chapel Hill (UNC), and Michigan State University (MSU).

REFERENCES

Agnello A., Kelly B. C., Treu T., Marshall P. J., 2015a, MNRAS, 448, 1446
Agnello A. et al., 2015b, MNRAS, 454, 1260
Alam S. et al., 2015, ApJS, 219, 12
Bertin E., Arnouts S., 1996, A&AS, 117, 393
Bolton A. S., Burles S., Koopmans L. V. E., Treu T., Moustakas L. A., 2005, ApJ, 624, L21
Bolton A. S., Burles S., Koopmans L. V. E., Treu T., Moustakas L. A., 2006a, ApJ, 638, 703
Bolton A. S., Moustakas L. A., Stern D., Burles S., Dey A., Spinrad H., 2006b, ApJ, 646, L45
Chan J. H. H., Suyu S. H., Chiueh T., More A., Marshall P. J., Coupon J., Oguri M., Price P., 2015, ApJ, 807, 138
Coles J., 2008, ApJ, 679, 17
Comerford J. M., Haiman Z., Schaye J., 2002, ApJ, 580, 63
Dahle H. et al., 2013, ApJ, 773, 146
Dahle H., Gladders M. D., Sharon K., Bayliss M. B., Rigby J. R., 2015, ApJ, 813, 67
Dawson K. S. et al., 2013, AJ, 145, 10
de Vaucouleurs G., 1948, Ann. Astrophys., 11, 247
Eisenstein D. J. et al., 2011, AJ, 142, 72
Falco E. E. et al., 1999, ApJ, 523, 617
Gunn J. E. et al., 2006, AJ, 131, 2332
Hennawi J. F. et al., 2006a, AJ, 131, 1
Hennawi J. F. et al., 2006b, ApJ, 651, 61
Hennawi J. F. et al., 2010, ApJ, 719, 1672
Hopkins P. F., Cox T. J., Kereš D., Hernquist L., 2008, ApJS, 175, 390
Inada N., 2012, AJ, 143, 119
Inada N. et al., 2008, AJ, 135, 496
Inada N. et al., 2009, AJ, 137, 4118
Inada N. et al., 2010, AJ, 140, 403
Jester S. et al., 2005, AJ, 130, 873
Johnston D. E. et al., 2003, AJ, 126, 2281
Kashikawa N. et al., 2002, PASJ, 54, 819
Kayo I., Oguri M., 2012, MNRAS, 424, 1363
Kochanek C. S., 1996, ApJ, 466, 638
Kochanek C. S., Falco E. E., Muñoz J. A., 1999, ApJ, 510, 590
Lang D., Hogg D. W., Mierle K., Blanton M., Roweis S., 2010, AJ, 139, 1782
McGreer I. D. et al., 2010, AJ, 140, 370
Mosquera A. M., Kochanek C. S., Chen B., Dai X., Blackburne J. A., Chartas G., 2013, ApJ, 769, 53
Myers A. D., Richards G. T., Brunner R. J., Schneider D. P., Strand N. E., Hall P. B., Blomquist J. A., York D. G., 2008, ApJ, 678, 635
Oguri M., 2010, PASJ, 62, 1017
Oguri M., Marshall P. J., 2010, MNRAS, 405, 2579
Oguri M. et al., 2006, AJ, 132, 999
Oguri M. et al., 2008, AJ, 135, 512
Oguri M. et al., 2012, AJ, 143, 120
Oke J. B. et al., 1995, PASP, 107, 375
Pâris I. et al., 2014, A&A, 563, A54
Peng C. Y., Ho L. C., Impey C. D., Rix H.-W., 2002, AJ, 124, 266
Peng C. Y., Impey C. D., Rix H.-W., Kochanek C. S., Keeton C. R., Falco E. E., Lehár J., McLeod B. A., 2006, ApJ, 649, 616
Peng C. Y., Ho L. C., Impey C. D., Rix H.-W., 2010, AJ, 139, 2097
Refsdal S., 1964, MNRAS, 128, 307
Richards G. T. et al., 2006, AJ, 131, 49
Ross N. P. et al., 2012, ApJS, 199, 3
Rusu C. E. et al., 2015, preprint (arXiv:e-prints)
Schechter P. L. et al., 1997, ApJ, 475, L85
Shen Y. et al., 2010, ApJ, 719, 1693
Smee S. A. et al., 2013, AJ, 146, 32
Suyu S. H., Marshall P. J., Auger M. W., Hilbert S., Blandford R. D., Koopmans L. V. E., Fassnacht C. D., Treu T., 2010, ApJ, 711, 201
The Dark Energy Survey Collaboration 2005, preprint (astro-ph/0510346)
Treu T. et al., 2013, preprint (arXiv:1306.1272T)
York D. G. et al., 2000, AJ, 120, 1579

This paper has been typeset from a TEX/LATEX file prepared by the author.